Absorption and Photocatalytic Degradation of VOCs by Perfluorinated Ionomeric Coating with TiO_2 Nanopowders for Air Purification

Maurizio Sansotera[a,b,†], Sina Geran Malek Kheyli[a,†], Alberto Baggioli[a,b], Claudia L. Bianchi[c], Maria Pia Pedeferri[a,b], Maria Vittoria Diamanti[a,b,*], Walter Navarrini[a,b]

[a] Dipartimento di Chimica, Materiali e Ingegneria Chimica, Politecnico di Milano, Via L. Mancinelli 7, 20131 Milan, Italy

[b] INSTM - Consorzio Interuniversitario Nazionale per la Scienza e Tecnologia dei Materiali (UdR-PoliMi), via G. Giusti, 9, 50121 Florence, Italy

[c] Dipartimento di Chimica, Università degli Studi di Milano, Via C. Golgi 19, 20133 Milan, Italy

* Corresponding author. Tel: +39.02.2399.3037; Fax: +39.02.2399.3280; Email address: mariavittoria.diamanti@polimi.it

[†] Equally contributing first authors: Maurizio Sansotera, Sina Geran Malek Kheyli

Abstract

In this work, we propose a transparent multilayered perfluoropolymeric coating as immobilization method for TiO_2 nanoparticles, and evaluate its suitability in the gas phase photocatalytic degradation of six different volatile organic compounds. The coating was made of a layer of TiO_2-containing perfluorosulfonic acid polymer on a layer of perfluorinated amorphous polymer. The chemical stability of perfluoropolymeric materials to UV radiation and UV-activated TiO_2 overcomes the possible degradation of the polymeric immobilization system which is typical of

more traditional polymeric coatings. Moreover, the TiO_2-containing ionomeric perfluorosulfonic layer worked as selective membrane for pollutants absorption and catalyst preservation, depending on the interactions between the superacidic polar heads of the ionomer and the pollutants, in particular those capable of hydrogen bonding. Gas-phase photocatalytic degradation tests were performed using pentane, methanol, 2-propanol, toluene, dichloromethane and pyridine as reference volatile organic pollutants, thus ranging on different polarity properties. Results indicate performances comparable to other approaches reported in the literature and show a strong influence of both atmospheric conditions (namely, humidity) and pollutant nature – polarity, proticity – on the actual kinetics of photodegradation, also depending on the interactions regulating the affinity between the ionomeric layer of the coating and pollutants. The high potential of the coating in the photodegradation was confirmed by the observed values of the photoabatement rates: all approximatively above 10^{-5} s^{-1} and maximum for alcohols (1.4×10^{-4} and 1.7×10^{-4} s^{-1} in dry and humid conditions, respectively).

Keywords: Photocatalysis; Gas phase; Volatile Organic Compounds; Titanium dioxide; Fluorinated PFSA coating

1 Introduction

Air pollutants have influence on comfort and life, and volatile organic compounds (VOCs) can generate adverse effects on human health by causing illnesses of increasing severity from sick building syndrome (SBS) [1-7] to cancer [8]. Thus, many people are nowadays victims of poor air quality and efficient technologies for VOC abatement are highly required [9]. Most standard depollution systems are based on filtration and absorption, requiring periodic replacement

[10].However, these systems showed that absorbed pollutants can still produce secondary VOCs, with supplementary risks for the human health [11].

Many advanced technologies like biological methods (biofilter, biotrickling filter, membrane bioreactor and bioscrubber) [12], plasmochemical systems [13] and advanced oxidation processes [14] have recently been developed for a quick and inexpensive removal of VOCs from air. Among these techniques, photocatalytic oxidation arises as a safe and advantageous method for the complete degradation of contaminants by exploitation of solar radiation [15-21]. Titanium dioxide, TiO_2, thanks to its high photocatalytic activity, lack of toxicity, chemical stability, and relatively low cost, is certainly the most studied photocatalyst and the focus of numerous well-established applications [22-25]. UV activation of TiO_2 can induce the formation of strongly oxidizing reagents, such as OH• radicals (redox potential $OH•/H_2O$ = +2.27 eV vs. the SHE) and O_2^{-}• superoxide ions (redox potential O_2/O_2^{-}•= -0.28 eV vs. the SHE), which can cause the decomposition of pollutants present in the air or water; in case of highly adsorbed pollutants, direct oxidation at the hole site of TiO_2 photocatalyst is also favored [25-27].

Several issues pertinent to the use of TiO_2 as photocatalyst in the form of conventional powders emerged during preliminary applications: for example, inefficient light exploitation, stirring difficulties during reaction, complex catalyst separation after reaction as well as concerns about the safe use of nanosized compounds [28-30]. TiO_2 immobilization inside a UV transparent solid matrix can overcome the aforementioned disadvantages [31-34]. However, the exposure of TiO_2 to UV light generates free radicals, which can degrade hydrogenated and partially halogenated polymers, such as polyvinyl chloride, polystyrene, polyvinyl alcohol, and polyethylene [35-38]. The compatibility of fluorinated materials in the presence of TiO_2 was also studied and perfluoropolymers resulted extraordinarily stable toward UV-activated TiO_2 photodegradation

[39]. In particular, amorphous perfluoropolymers showed the highest chemical stability and, due to their high UV transparency and high gas permeability, emerged as best candidate class of materials for the fabrication of TiO_2-embedding matrices [40,41]. Recently, a multilayered perfluorinated coating based on amorphous and low-crystalline fluoropolymers with immobilized TiO_2 was applied in a continuous photocatalytic apparatus for water remediation [42]. In this application, the multilayered coating comprised an ionomeric layer of perfluorosulfonic acid (PFSA) polymer in order to optimize the interaction between the catalyst and the polluted aqueous solution [42].

Although TiO_2-mediated photocatalysis is the subject of a very large number of research studies, it is difficult to find a comprehensive account addressing a large number of pollutants: in general, only one model reactant is considered, which is not necessarily representative of the actual photocatalytic efficiency of the material against other pollutants. Moreover, while several immobilization methods have been proposed to produce stable photocatalytic coatings for water purification [43-45], in gas phase photocatalysis the catalyst nanoparticles are generally spread on a suitable support, or alternatively produced by sol-gel and applied by spraying or dipping [45-48]. This poses some questions on the actual stability of the coating and on the potential dispersion of nanoparticles in the treated air effluent, with related health concerns, and opens the way to scientific research on reliable and efficient methods of catalyst immobilization.

In the present work, the photocatalytic activity of a TiO_2-containing perfluorinated coating was tested against six different gas-phase VOCs, chosen for their environmental effects and for screening a broad range of polarity properties. The selected pollutants are pyridine, pentane, methanol, 2-propanol, toluene, and dichloromethane. Pyridine is highly polar, has alkaline behavior and, despite its wide use as industrial solvent, it is extremely harmful to human organs,

such as liver, kidney, nerve system, and eyes, causing nausea, headache, insomnia, and other disorders [49,50]. Pentane is a completely apolar hydrocarbon and it is a colorless toxic liquid used in establishing the octane rating for gasoline, thus being released by gasoline evaporation [51]. Dichloromethane is a colorless, highly volatile toxic chlorohydrocarbon, widely used as solvent; as it belongs to chlorinated VOCs, it is often used as model molecule to investigate the behavior of this class of pollutants [52]. Methanol is a polar alcohol which can cause damage to several organs, particularly to the optic nerve. Nowadays there is a great interest in making methanol manufacturing more environmentally friendly because it is massively produced from syngas for application as hydrogen and energy carrier [53]. 2-propanol is an alcohol with lower polarity than methanol and it is also well known to cause ocular surface irritation, epithelial keratitis and occasionally corneal abrasion [53]. Finally, toluene belongs to the class of aromatic hydrocarbons and it is a model compound which provides useful information for its treatment and for dealing with more complicated organic pollutants [54].

2 Materials and methods

2.1 Coating materials

Aquivion® D83-06A (AQ) and Hyflon® AD60 (AD)(Solvay Specialty Polymers) were employed for the preparation of the photoactive coating. AQ is a melt-extruded ionomeric branched copolymer, obtained from tetrafluoroethylene (TFE) and a sulfonyl fluoride vinyl ether (SFVE), $F_2C{=}CF{-}OCF_2CF_2SO_2F$: the starting material is in the acidified form, in a 6% solution of 1-propanol (40%), 2-propanol (40%) and water (20%). Namely, AQ was the PFSA polymer employed for embedding the catalyst particles. AD is a random copolymer of TFE and 2,2,4-trifluoro-5-trifluoromethoxy-1,3-dioxole (TTD), characterized by outstanding chemical stability,

low refractive index (equal to 1.327) and T_g of 130ºC [41].For the experimental tests, AQ was used as received and AD was dissolved in solution by using Galden® HT110 (Solvay Specialty Polymers) as solvent. Galden® HT110 is a PFPE-based solvent with boiling point of 110ºC and formula as follow: $CF_3O(CF_2CF(CF_3)O)_p(CF_2O)_nCF_3$ ($p+n$ = 2-3; p/n = 20-50).

Nanometric powder of commercial titanium dioxide P25 (75% anatase, 25% rutile, Evonik®) with a band gap between 3.05 and 3.15 eV was employed as a photocatalyst [55].

2.2 Photocatalytic apparatus

The photochemical apparatus consisted of a Pyrex® glass reactor (internal volume: 145 ml) covered with a quartz glass, irradiated with a Ultra Vitalux® lamp (Fig. 1 and Fig. S.I.-1 in the Supporting Information). The insertion of pollutants and water, as well as for the collection of gas samples for GC-MS analyses, was performed through a septum positioned at half cell height. The reactor contained a stirring device for the homogenization of gases inside the reactor. Tests were performed in batch conditions.

The lamp employed is well known in photocatalytic tests, since it is a widely used broad spectrum lamp. The UV irradiation intensity was 21 mW/cm^2, as measured by means of a UM-10 Konica Minolta radiometer. Tests were performed both at high temperature (85°C) and at room temperature (approx. 20°C): the temperature profile in the reactor was monitored by means of a thermocouple, in order to ensure a constant temperature throughout the whole test duration.

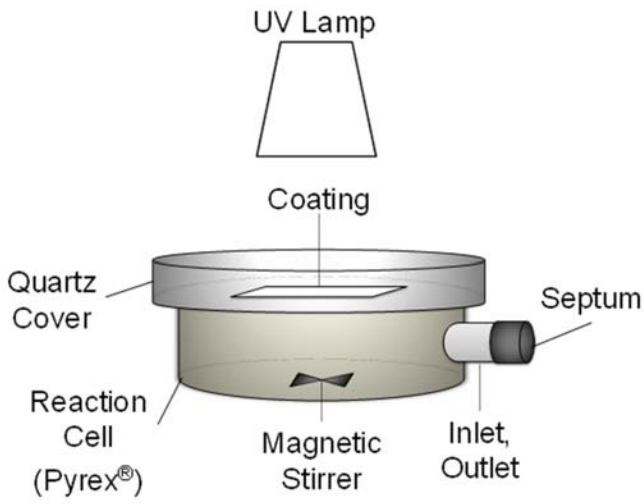

Figure 1. Experimental apparatus.

2.3 Photoactive coatings production

The deposition of an endurably stable photoactive coating on the quartz cover of the reactor was obtained by applying a first layer of AD, followed by thermal curing and application of a second layer of AQ, containing the photocatalyst nanoparticles. A 10 wt% solution of AD in Galden® HT110 [56] and a 6% solution of AQ in a hydroalcoholic solvent (water/*i*-propanol/*n*-propanol 20:40:40) containing 0.6 wt% of dispersed active nanometric TiO_2 (*i.e.*, 10 wt% of TiO_2 on AQ content) were employed. The former acted as inner hydrophobic fluorinated primer, in contact with glass, and the latter as outer photoactive layer. Both polymeric AD and AQ layers were chemically stable toward the degradation effects due to UV light and TiO_2 photocatalytic activity [40].

The fine dispersion of TiO_2 in the hydroalcoholic AQ solution was obtained by ultra-sonication for 40 min at room temperature in order to homogenize the catalyst into the ionomeric mixture.

The AD layer was thermally cured for 1 h under N_2 flux and 1 h under vacuum at 50°C, and then after adding the AQ layer, the whole coating was thermally cured for 1 h under N_2 flux at the same

temperature. Since P25 photocatalyst can suffer conversion to rutile phase only at high calcination temperatures, we assumed that the thermal curing of AQ polymeric layer did not affect TiO_2 phase and band gap [57]. The average weights of the AQ and AD layers were 12±3 mg and 25±3 mg, respectively, and the size of the photoactive coatings on the quartz cover of the reactor was 3.5×3.5 cm^2.Overall, the multilayered photocatalytic coating resulted adherent to the internal surface of the quartz cover of the reactor and it was in direct contact with the gaseous pollutants.

For benchmarking purposes, two photoactive coatings made of a single layer of pure fluoropolymer containing TiO_2 were prepared: one AQ-based and one AD-based coating. The former was thermally cured for 1 h under N_2 flux at 50°C, and the latter was thermally cured for 1 h under N_2 flux and then for 1 h under vacuum at 50°C.

2.4 Model reactants for photocatalysis tests

Table 1. Chemical formula, polarity and volumes of liquid VOC pollutants injected in the reactor in order to obtain reference gas-phase concentrations of 5000 and 2000 ppm.

Name	Chemical Formula	Dipole Moment (D)	5000 ppm V (µl)	2000 ppm V (µl)
Pentane	C_5H_{12}	0	3.7	1.5
Toluene	C_7H_8	0.37	3.4	1.4
2-propanol	C_3H_7OH	1.56	2.5	1.0
Dichloromethane	CH_2Cl_2	1.60	2.1	0.8
Methanol	CH_3OH	1.70	1.3	0.5
Pyridine	C_5H_5N	2.21	2.6	1.0

As previously mentioned, tested pollutants were chosen with increasing dipole moment and on the basis of their environmental interest (Table 1). The volumes of the volatile liquid pollutants

injected in the reactor in order to obtain the reference gas-phase concentrations of 5000 and 2000 ppm are reported in Table 1.

2.5 Coatings characterization

All the photoactive coatings were first characterized by static contact angle measurements with different liquids (*i.e.*, water, *n*-hexadecane, squalane, *n*-perfluorohexane) and their surface energy was calculated on the basis of the theory of equation of states. The contact angle instrument used in this analysis is Data Physics OCA 150 and the software is SCA20 version 2.3.9. build 46.

The X-ray photoelectron spectroscopy (XPS) spectra were obtained by using an M-probe spectrometer manufactured by Surface Science Instrument. The spectra were excited with monochromatic X-ray emission A1 Kα radiation (1486.6 eV). A spot size of 300×300 μm and pass energy of 29 eV was used. *1s* level hydrocarbon-contaminant carbon was taken as the internal reference at 284.6 eV. Fittings were performed using pure Gaussian peaks, Shirley's baseline, and without any constraints. Transmission electron microscopy (TEM) was performed by using a Philips CM200 electron microscope operating at 200 kV equipped with a Field Emission Gun filament (FEI Company, Eindhoven, The Netherlands). Scanning electron microscopy (SEM) was employed to analyze the morphology of MW-CNTs samples. Microscopy was performed with a Zeiss EVO–50 (working distance 8.0 mm, beam current 100 pA, acceleration voltage 20.00 kV) on bare samples without deposition of a conductive layer. X-ray diffraction (XRD) patterns were obtained with thin film configuration on a Philips PW 1830 X-ray Diffractometer equipped with a Philips PW 3020 Goniometer with Cu Kα radiation (λ = 1.54058 Å) at a scan rate of 0.02° s^{-1}.

The photocatalytic activity of the TiO_2-embedded perfluorinated ionomeric coatings was evaluated by monitoring ratio between the concentration of each pollutant at different times of irradiation

and its initial concentration *via* GC-MS analysis. An Agilent GC-MS system 6850-5975C with a Poraplot U column was used throughout.

Photocatalysis (**Pc**) tests were performed in the presence of the photoactive coating under UV irradiation. Since humidity influences the hydration of the PFSA-based ionomeric layer in the photocatalytic coating, **Pc** tests were performed at 85°C, and at two relative humidities (RH): in dry conditions at ~20% RH (**Pc-D** test) and in wet conditions with content of water corresponding to a 5-fold saturated air, namely 500% RH (**Pc-W** test).

The absorption properties of the coating were evaluated in dark tests (*i.e.*, **Abs** tests) in the presence of the photoactive coating. Three different **Abs** tests were performed for each pollutant: at room temperature (RT) in dry conditions (**Abs-RTD** test), at 85°C in dry conditions (**Abs-85D** test) and at 85°C in wet conditions (**Abs-85W** test). Absorption in wet conditions was slightly enhanced at RT with respect to what observed at 85°C, being the observed kinetic constants equal to 9.6 and 7.3×10^{-6} s^{-1}, respectively (see Supporting Information). In the following, only room temperature absorption will be shown for the sake of simplicity: this condition was chosen as it provides the worst benchmark for photocatalysis tests, being a higher share of decrease in pollutant concentration ascribed to absorption rather than to photocatalysis.

It is worth underlining that absorption tests reflect the ability of the coating as a whole to absorb the pollutant, facilitating its diffusion towards the photocatalyst nanoparticles embedded in the coating, rather than the pollutant direct adsorption on the surface of the photocatalyst.

Finally, photolysis tests were also carried out by treating the pollutants under UV irradiation in the absence of the photoactive coating (*i.e.*, **Pl** tests). All measured data of concentrations of pollutants in time are reported in the Supporting Information.

Absorption, photocatalytic and photolytic reactions were considered to follow pseudo-first order kinetics (correlation coefficient $R^2 > 0.9$) which enabled the direct comparison of the apparent rate constants (k_{app}), calculated as follows:

$$lnC/C_0 = -k_{app}\, t$$

where C and C_0 are the pollutant concentration at time t and at the beginning of the test, respectively, and t is reaction time.

3 Results

3.1 Photocatalytic coating assembly and preliminary characterization

In this work, two amorphous perfluoropolymeric materials were considered for the fabrication of a photocatalytic coating tested on the TiO_2-catalyzed abatement of pollutants in gas phase: ionomeric AQ and high-T_g AD, which is a TFE-TTD copolymer. Both fluoropolymers can be used in this application because they are characterized by high transparency, particularly in the UV region, and complete stability toward UV radiation and reactivity of UV-activated TiO_2. In the early stage of this research, three different photocatalytic coatings with embedded TiO_2 were prepared for comparison: a single layered coating of AQ, a single layered coating of AD and a multilayered photoactive coating obtained by depositing an AQ layer on an AD layer (AQ-AD coating).

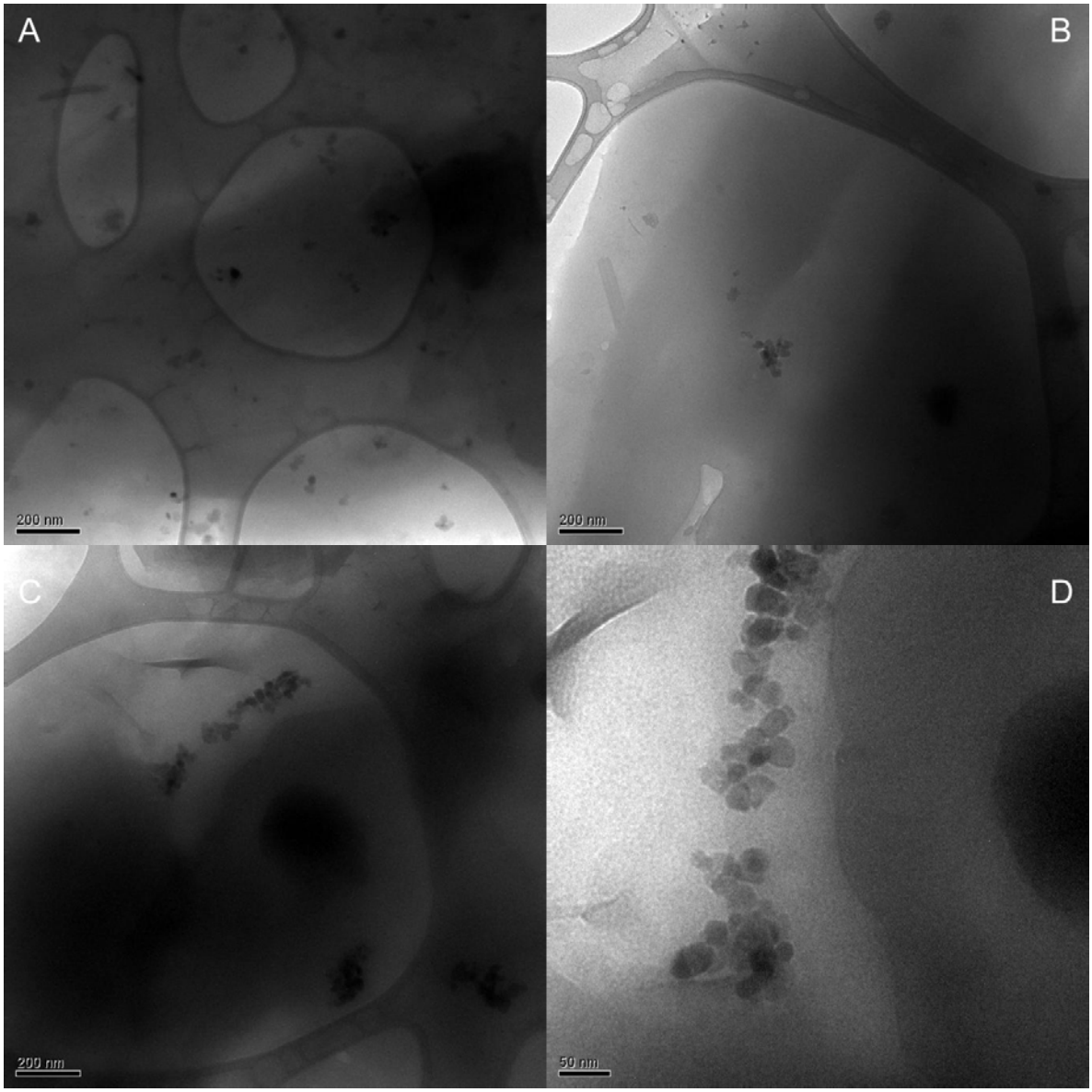

Figure 2. TEM micrographs of several spots of the AQ-AD multilayered coating (A, B and C) and high magnification micrograph on a nanometric aggregate of TiO_2 (D).

These photocatalytic coatings were characterized by SEM, TEM and XRD in order to define their morphological and structural characteristics. Figure 2 reports the TiO_2 nanoparticles dispersion in the polymeric coating as observed by TEM. It is possible to notice that TiO_2 nanoparticles were distributed within the fluoropolymeric coating as agglomerates generally having sizes in the order

of a hundred nanometers. Yet, some larger cluster, of more than 1 μm size, were also identified in the coating by SEM observations (see Supplementary Information, Fig. S.I.-2). Thus, the photoactive layer of the coating embedded micrometric TiO_2 clusters that were surrounded by ionomeric polymer in which TiO_2 nanoparticles were randomly dispersed. XRD analyses confirmed the crystallinity of the TiO_2 nanoparticles, with co-existence of anatase and rutile phases, in agreement with the typical crystal structure of P25 nanopowders [55] (Fig. S.I.-3).

Table 2. Static contact angle with different liquids (water, *n*-hexadecane, squalene and *n*-perfluorohexane) on different coatings and their corresponding surface energies.

Photoactive coating	**Static contact angle[a]**				**Surface energy (mN/m)**
	water	***n*-hexadecane**	**squalane**	***n*-perfluorohexane**	
AQ-based	62°±3°[b]	29°±1°	40°±2°	9°±1°	33.0
AD-based	110°±2°	54°±1°	59°±2°	12°±4°	16.5
AQ-AD multilayer	45°±3°[b]	28°±1°	34°±4	8°±1°	39.5

a. static contact angles were measured after exposing the samples to an environment at 20% RH for 6 h.
b. immediately after the curing treatment, both AQ- and AQ-AD-coatings showed a contact angle equal to 85°±3°, corresponding to a surface energy of 26.0 mN/m (±0.3 mN/m).

On all of the previously defined photocatalytic coatings (AQ-based, AD-based and multilayer), static contact angle measurements with four different liquids: water, *n*-hexadecane, squalene, and *n*-perfluorohexane (Table 2). The AD-based coating showed the lowest wettability with a surface energy around 16.5 mN/m, due to high hydrophobicity and to the most marked oleophobicity in the series. The single layered AQ-based coating and the multilayered AQ-AD coating freshly extracted from the N_2 atmosphere of the curing treatment, hence fully dry, resulted similar, with a surface energy for both equal to 26.0 mN/m. However, after exposing the coatings to a slightly moisturized environment (RH = 20%), the AQ-AD coating revealed a surface energy higher than

that of the single layered AQ-based coating: 39.5 and 33.0 mN/m, respectively (Table 2). These different wettabilities can be ascribed to a quicker absorption of humidity in the multilayered coating, due to the surface-oriented assembly of the polar sulfonic moieties driven by fluorophilic interactions between the AD layer and the fluoropolymeric AQ backbone.

Table 3. Surface composition (at%) of the components of AQ-AD multilayered coating embedding TiO_2 photocatalyst.

Samples	Amount (at%)							Ti/S	CF/C_{tot}[a]
	F	O	C	S	N	Si	Ti		
AQ	54.8	8.7	32.6	1.6	1.2	1.1	-	-	0.69
AD	52.7	17.1	30.2	-	-	-	-	-	0.92
TiO_2	-	48.5	34.1	-	-	-	17.4	-	-
AQ-AD multilayer	55.8	6.8	33.5	1.9	1.6	-	0.4	0.21[b]	0.75

a. CF/C_{tot} ratio was obtained by dividing the areas of the deconvolutions attributed to fluorinated moieties on *C 1s* region by the total area of all the deconvolutions in the same region (see Fig. S.I.-4 in the Supporting Information).
b. 1.04 is the Ti/S ratio based on the composition of the starting solution with 6% of AQ in hydroalcoholic solvent containing 0.6 wt% of nanometric TiO_2.

XPS data are reported in Table 3; spectra of relevant regions are also reported in the Supplementary Information section (Fig. S.I.-4 and S.I.-5). The highly fluorinated nature of AQ and AD is preserved in the multilayered coating. Moreover, the presence of sulfur in both pure AQ (1.6 at%) and AQ-AD multilayer (1.9 at%) confirmed that the deposition process prevented the mixing of the two fluoropolymers and maintained the ionomeric moieties on the surface of the final coating. The Ti/S ratio, correlated to the amount of TiO_2 per PFSA group in the AQ layer, on the surface of the AQ-AD multilayered coating showed a value equal to 0.21. This value resulted significantly lower than 1.04, which is the value obtained from the composition of the starting solution of AQ containing the dispersion of nanometric TiO_2. This behavior can be explained supposing that the TiO_2 migrated preferentially in the bulk of the AQ layer of the coating, rather than staying on the

surface, or, alternatively, that part of TiO_2 was dispersed during the deposition process. The high resolution spectrum in the Ti *2p* region of the AQ-AD coating embedding TiO_2 (Fig. S.I.-4D) showed a typical pattern ascribable to pure nanometric TiO_2, ascertaining the idea that the photocatalyst was not influenced by the surrounding environment made of the PSFA-based polymer. Oxygen peaks were also analyzed [58,59], showing that the signals of oxygen in the AQ membrane and in the TiO_2 containing multilayer coating coincide (Fig. S.I.-5). This proves the stability of the AQ layer and its positioning on the outer side of the multilayer coating, confirming that AQ is still the final coating layer exposed to the environment also after the annealing treatments required for the stabilization of the photoactive coating.

The photocatalytic properties of the three coatings were also compared: this was done by monitoring the abatement of pentane in wet conditions under UV exposure with an initial concentration of the pollutant equal to 5000 ppm. Pentane was chosen within the pollutants list because it resulted particularly resistant to photocatalytic abatement in preliminary tests and, therefore, it was a suitable reference molecule for performances differentiation. Moreover, as it will be discussed in greater detail in the next paragraph, the apolar character of pentane is at the basis of its negligible affinity toward the AQ layer, therefore its absorption is very low and independent on coating hydration. Thus, all the differences observed in this specific test (Fig. 3) can be ascribed to the actual influence of relative humidity on the photocatalysis mechanism, and not on pollutant absorption.

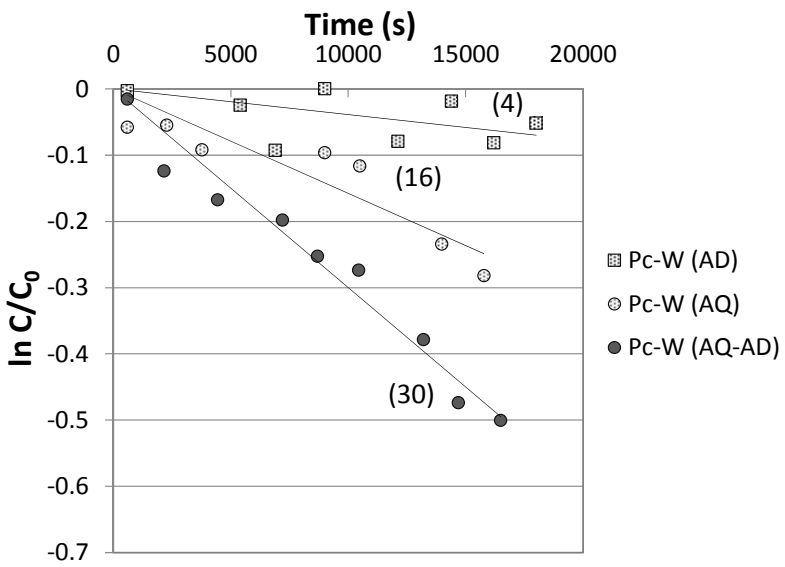

Figure 3. Photocatalytic abatement of pentane in wet conditions (**Pc-W** test) with three different photoactive coatings with embedded TiO_2: AQ-based coating (dotted circle), AD-based coating (dotted square) and multilayered AQ-AD coating (grey circle). Apparent rate constant values (k_{app}) are reported in brackets (values × $10^{-6}s^{-1}$).

As reported in Figure 3, the most performing pentane photocatalytic abatement was obtained by employing the multilayered AQ-AD coating: in wet conditions a rate constant equal to 30 × 10^{-6} s^{-1} was measured. Single layered AQ coating showed intermediate activity (16 × 10^{-6} s^{-1}), while AD-based coating nearly inhibited photodegradation (4 × 10^{-6} s^{-1}). The ionomeric nature of the PFSA AQ polymer favored both the direct oxidation of highly absorbed molecules at TiO_2 hole sites and the hydroxyl radical mediated degradation of weakly absorbed pollutants on the coating surface. In the multilayered AQ-AD coating the pollutant absorption was furtherly facilitated by the preferential orientation of the ionomeric AQ moieties toward the surface induced by the underlying AD layer. In the AD-based coating both the high hydrophobicity and the oleophobicity

of the amorphous AD fluoropolymer almost blocked the direct oxidation pathway and only a weak degradation of the pollutant due to hydroxyl radical reactivity was observed.

Based on contact angle measurements and pentane abatement results, the multilayered AQ-AD photoactive coating resulted the most promising for further development and, therefore, the study of RH influence on oxidation rate and the tests on photodegradation of other pollutants were focused on this multilayer coating system.

3.2 Effect of relative humidity

The hydration level of the PFSA ionomer-based layer, *i.e.* AQ layer, embedding TiO_2 catalyst can widely influence the permeation rates of pollutant molecules in the multilayered AQ-AD coating [60,61]. Moreover, the role of water molecules in the mechanism of photo-induced oxidation catalyzed by TiO_2 is widely recognized [62-64]. Since in gas-phase reactions the water content can range from dry to wet conditions depending on the reaction environment, a preliminary evaluation of the effects of environmental humidity on VOC abatement rates was performed. Also in this case, pentane was employed as target pollutant: a dry condition with ~20% RH and three different wet conditions were selected, with water additions corresponding to 3-fold, 5-fold and 16-fold air saturation. The oversaturated conditions were considered because part of the water can be absorbed by the AQ layer during the reaction and the corresponding value of oversaturation was referred to the amount of water added in the reaction chamber at the beginning of the experiments.

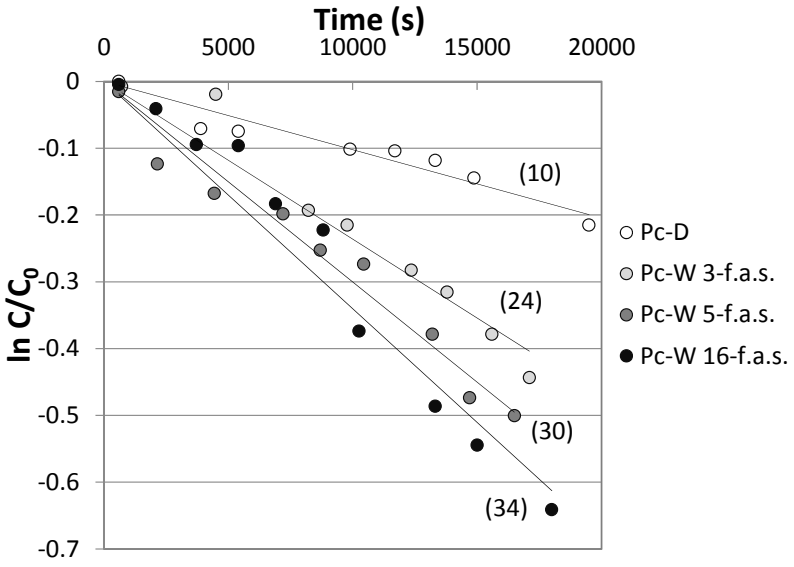

Figure 4. Photocatalytic abatement of pentane in dry (white) (**Pc-D**) and wet conditions (**Pc-W** tests) with three different water contents: 3-fold (light-grey), 5-fold (dark-grey) and 16-fold (black) air saturation (labeled as 3-, 5- and 16-f.a.s., respectively). Apparent rate constant values (k_{app}) are reported in brackets (values × $10^{-6}s^{-1}$).

In dry conditions (**Pc-D** test) pentane was photocatalytically decomposed with a k_{app} equal to 10 × 10^{-6} s^{-1}, which was the lowest observed apparent rate constant in the tests at different RHs (Fig. 4). The increase in atmospheric humidity progressively increased the photodegradation rates: in conditions of 3-fold, 5-fold and 16-fold air saturation, the k_{app} were 24 × 10^{-6}, 30 × 10^{-6} and 34 × 10^{-6} s^{-1}, respectively (Fig. 4). Humidity enhanced the hydration of polar ionomeric moieties of AQ and, thus, it improved the availability of water-filled ionic cluster channels surrounded by fluoropolymeric AQ phase [65-67]. As a consequence, the hydration of AQ ionic clusters increased the absorption of the pollutants inside the ionomeric layer and the degradation was performed by both bulk and surface TiO_2 photocatalyst particles. Based on this principle, the TiO_2-catalyzed photoabatemet of pentane resulted approximately from 2.5 to 3.5 times more efficient in wet

conditions than in dry conditions. However, the improvements due to high RH almost reached stability passing from 5-fold to 16-fold water saturation: despite an augmentation of 3 times in water content, the photodegradation rate increased only by 13%.

The addition of water corresponding to a 5-fold supersaturation of the reaction environment, namely 500% RH, was employed as optimized condition in the photocatalytic abatement tests with toluene, 2-propanol, dichloromethane, methanol, and pyridine. Absorption rates in this condition were also evaluated.

3.3 Absorption and photocatalysis

The photocatalytic performances of the multilayered AQ-AD photoactive coating were evaluated by comparing the abatement of several pollutants, such as pentane, toluene, 2-propanol, dichloromethane, methanol, and pyridine, in a condition of 5-fold water oversaturation of the reaction environment. In the multilayered AQ-AD assembly, the AQ layer resulted directly exposed to the reactor chamber. Thus, it was expected that the gaseous pollutants were adsorbed on the AQ layer and diffused within it until reaching the embedded TiO_2 photocatalyst particles. Perfluorinated ionomers with strongly acid sulfonic moieties, like AQ, can exhibit phase-transfer capabilities related to the continuous water phase clusters formed inside the hydrophobic fluorinated matrix [68]. Molecular oxygen can also penetrate into the photoactive coating due to the high gas permeability of the AQ polymer [69]; then, in the presence of UV light and oxygen, pollutants can be oxidized by photoactivated TiO_2 particles or by TiO_2-generated radical species (like hydroxyl radicals and superoxide ions), achieving their mineralization or generating partially oxidized intermediates and by-products [70].

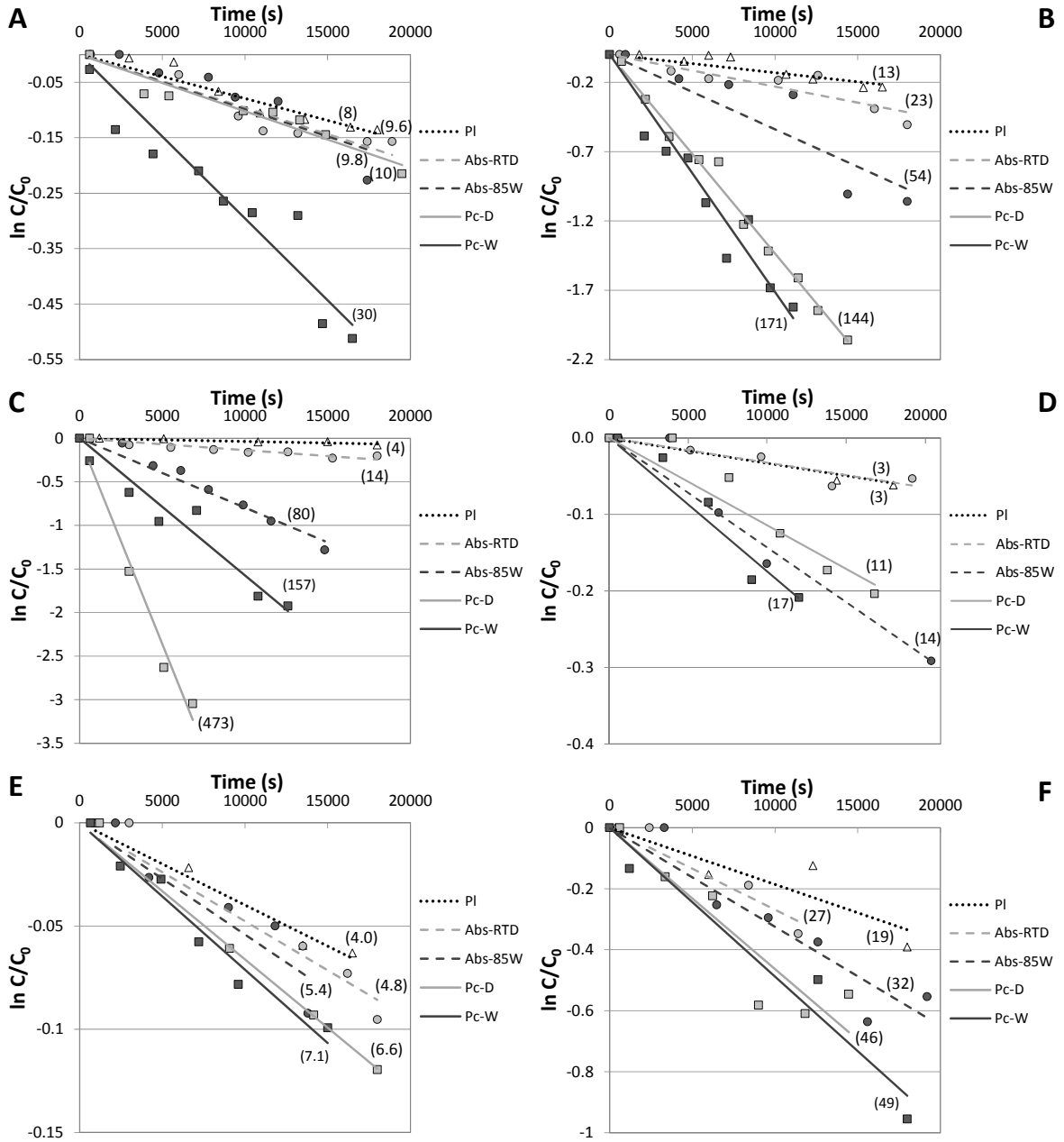

Figure 5. Photolysis (white triangle, linearized with dotted line), absorption in dry (light grey circle, linearized with light grey dashed line) and wet (dark grey circle, linearized with dark grey dashed line) conditions and photocatalytic abatement in dry (light grey square, linearized with light grey solid line) and wet (dark grey circle, linearized with dark grey solid line) condition of pentane (**A**), methanol (**B**), 2-propanol (**C**), toluene (**D**), dichloromethane (**E**) and pyridine (**F**).

Apparent rate constant values (k_{app}) are reported in brackets (values × $10^{-6}s^{-1}$). In Fig. 5C the value of Pc-D (473 × 10^{-6} s^{-1}) is overestimated due to competitive synthesis of propene.

Degradation reactions and absorption phenomena appeared to follow pseudo-first order kinetics, enabling the comparison of the corresponding apparent rate constants (k_{app}).

Pentane, C_5H_{12}, was tested as apolar volatile hydrocarbon pollutant and its mineralization reaction is shown below (eq. 1):

$$C_5H_{12} + 8\ O_2 \rightarrow 5\ CO_2 + 6\ H_2O \qquad (1)$$

Due to the lack of affinity between apolar hydrocarbons and ionomeric AQ layer, it was expected that pentane absorption in the photocatalytic layer would be hindered, without significant variations ascribable to coating hydration. Experimental data confirmed this behavior (Fig. 5A). Pentane absorption in dry conditions at room temperature (**Abs-RTD**) as well as in wet conditions at 85°C (**Abs-85W**) showed low apparent kinetic rate constants with similar values: 9.6 × 10^{-6} and 9.8 × 10^{-6} s^{-1}, respectively. Thus, the hydration of the photocatalytic layer resulted nearly irrelevant on absorption rates of pentane. Moreover, pentane photolysis (**Pl**) and photocatalysis in dry condition (**Pc-D**) showed very similar k_{app} equal to 8 × 10^{-6} and 10 × 10^{-6} s^{-1}, respectively. The photolytic mechanism, therefore, remained dominant also during the photocatalytic degradation test of pentane in dry conditions because the contact between pollutant molecules and photocatalyst particles was prevented by the actual absence of pentane absorption. The photocatalytic abatement of pentane in wet conditions (**Pc-W**) followed a different mechanism, related to the presence of water in AQ layer and the subsequent formation of strongly oxidizing species by UV-activation of TiO_2. In similar conditions, Shang *et al.* observed the formation of alcohol intermediates during the photocatalytic oxidation of alkanes with TiO_2 as photocatalyst

[71,72]. A similar scenario can also be envisioned in our case, considering the formation of oxidizing species at the TiO_2 surface and their transport through the coating to the coating/atmosphere interface, where they react with pentane. The free-radical synthesis of hydroxylated species derived from pentane can be summarized in the following scheme, in which H_2O_{ads} represents water molecules absorbed in the ionomeric layer and adsorbed on photocatalyst particles and h^+ photogenerated holes on TiO_2 surface (eq. 2-4):

$$H_2O_{ads} + h^+ \rightarrow \cdot OH + H^+ \quad (2)$$

$$C_5H_{12} + \cdot OH \rightarrow C_5H_{11}\cdot + H_2O \quad (3)$$

$$C_5H_{11}\cdot + H_2O \rightarrow C_5H_{11}(OH) + H\cdot \quad (4)$$

Once these polar alcoholic intermediates are formed, their absorption in the ionomeric layer becomes highly facilitated, allowing the direct contact with photoactivated TiO_2 particles. As a consequence, the apparent kinetic rate constant of the photocatalytic abatement of pentane in wet conditions (**Pc-W**) resulted the highest of the series (Fig. 5A): 30×10^{-6} s^{-1}.

Methanol permeability in PFSA membranes has been widely studied for application in direct methanol fuel cells [73-76]. It was demonstrated that methanol readily diffuses into PFSA polymers with permeation rates inversely proportional to the hydration of the membrane: in water-swelled PFSA specimens, almost no preferential absorption was observed between water and methanol [77-80]; conversely, water sorption resulted favored in dry PFSA specimen [81,82]. Moreover, mechanistic studies on the photocatalyzed oxidation of methanol suggest that, depending on water presence and O_2 concentration, direct or indirect oxidation reactions can competitively occur [83]. Formate and formaldehyde intermediates are considered as the primary products of direct and indirect oxidation reactions, respectively [83]. The complete oxidation reaction of methanol is here reported (eq. 5):

$$CH_3OH + 3/2\ O_2 \rightarrow CO_2 + 2\ H_2O \qquad (5)$$

Methanol photodegradation through the multilayered AQ-AD photoactive coating was evaluated taking into account the effects of hydration of the photocatalytic layer due to atmospheric humidity. The facilitation of methanol absorption due to hydration of the PFSA component of the photocatalytic layer was experimentally confirmed by determining the corresponding apparent kinetic rate constants (Fig. 5B): in dry conditions at room temperature (**Abs-RTD**) a value of 23 $\times 10^{-6}$ s^{-1} was observed, which raised to 54 $\times 10^{-6}$ s^{-1} in wet conditions at 85°C (**Abs-85W**). An analogous, although less pronounced, humidity-related increase was also observed in methanol photocatalytic reaction constants (Fig. 5B): k_{app} at 85°C resulted equal to 144 $\times 10^{-6}$ and 171 $\times 10^{-6}$ s^{-1} in dry (**Pc-D**) and wet (**Pc-W**) conditions, respectively. The hydration of the photocatalytic layer significantly influenced methanol absorption rate and, hence, the overall photocatalytic performances of the multilayered photoactive coating. Comparing direct and indirect oxidation reactions of methanol, the direct route was favored by the ready diffusion of this pollutant, which easily permeated inside the ionomeric AQ layer encountering the photocatalyst particles on which the abatement occurred. Because of the properties related to the carboxylic nature of formate, such as high polarity, high solubility in water and low vapor pressure, these intermediates of methanol direct oxidation remained absorbed in the bulk of the ionomeric layer, proceeding to a complete mineralization. Thus, detection of formate traces was not possible by GC-MS sampling of the gas-phase reaction environment during methanol photocatalytic abatement. Traces of monohydrated formaldehyde, namely methanediol, $CH_2(OH)_2$, were detected during the photocatalytic tests in wet conditions (**Pc-W**), confirming that the presence of water favored the indirect route of methanol oxidation.

2-propanol belongs to the class of alcohols and, due to the shortness of its carbon-based chain, its permeation in PFSA membranes is expected to be similar to that of methanol [84,85]. Moreover, 2-propanol abatement is an interesting issue because it is a typical volatile organic pollutant present in urban atmosphere and particularly in indoor environments [86,87]. There is agreement in the literature that the main gaseous products in TiO_2-catalyzed photooxidation of 2-propanol under UV light irradiation are acetone as intermediate (eq. 6) as well as CO_2 and H_2O as final products (eq. 7) [88,89]:

$$CH_3CH(OH)CH_3 + 1/2\ O_2 \rightarrow CH_3C(O)CH_3 + H_2O \qquad (6)$$

$$CH_3CH(OH)CH_3 + 9/2\ O_2 \rightarrow 3\ CO_2 + 4\ H_2O \qquad (7)$$

The formation of acetaldehyde and isopropyl formate traces has been also reported [87].

Gas-phase 2-propanol abatement by means of the multilayered AQ-AD photoactive coating was tested, considering also absorption facilitation due to the marked similarities between methanol and 2-propanol behaviors. Apparent kinetic rate constants of $14 \times 10^{-6}\ s^{-1}$ and $80 \times 10^{-6}\ s^{-1}$ were measured for 2-propanol absorption in dry conditions at room temperature (**Abs-RTD**) and in wet conditions at 85°C (**Abs-85W**), respectively (Fig. 5C). A further increment was observed in wet photocatalysis conditions (**Pc-W**), showing at 85°C a k_{app} of $157 \times 10^{-6}\ s^{-1}$ (Fig. 5C). During the photocatalytic test at 85°C in dry conditions (**Pc-D**) an extraordinary high k_{app} of $473 \times 10^{-6}\ s^{-1}$ was measured because in these conditions the competitive synthesis of propene due to 2-propanol dehydration (eq. 8) was also favored (Fig. 5C):

$$CH_3CH(OH)CH_3 \rightarrow CH_3CH{=}CH_2 + H_2O \qquad (8)$$

Propene formation was confirmed by GC-MS analysis of gas-phase samples collected during 2-propanol photocatalytic abatement. Hence, the anomalously high value of k_{app} should not be considered as a result of photocatalytic activity, but rather of propene synthesis.

Toluene is an important constituent of anthropogenic emissions in urban atmospheres and its photo-oxidation is a very demanding reaction that can be considered as a tough chemical test to assess the potential of TiO_2-based systems in the photo-elimination of organic pollutants [39,90-92]. In fact, the complete mineralization of toluene to carbon dioxide and water vapor (eq. 9) passes through the formation of deactivated intermediates, like benzaldehyde (eq. 10), benzoic acid (eq. 11) and benzene (eq. 12), and other highly stable side-products such as hydroxylated benzaldehydes (eq. 13) [91]:

$$C_6H_5CH_3 + 9\ O_2 \rightarrow 7\ CO_2 + 4\ H_2O \quad (9)$$

$$C_6H_5CH_3 + O_2 \rightarrow C_6H_5C(O)H + H_2O \quad (10)$$

$$C_6H_5C(O)H + ½\ O_2 \rightarrow C_6H_5C(O)OH \quad (11)$$

$$C_6H_5C(O)H + ½\ O_2 \rightarrow C_6H_6 + CO_2 \quad (12)$$

$$C_6H_5C(O)H + ½\ O_2 \rightarrow HO\text{-}C_6H_4C(O)H \quad (13)$$

The interactions between PSFA membranes and aromatic compounds have been discussed in a limited number of studies about the development of membrane electrolyzers for hydrogenation of aromatic compounds with water splitting [93-95]. Mitsushima *et al.* described an electrolyzer for toluene hydrogenation working with a conversion of 95%, under the assumption of a substantial absence of toluene permeation within the PFSA membrane [95]. The application of the multilayered AQ-AD photoactive coating to toluene abatement confirmed that toluene absorption in the PFSA layer was hindered in dry conditions (**Abs-RTD**) and a low apparent kinetic rate constant of 3×10^{-6} s^{-1} was observed (Fig. 5D). A k_{app} increase was observed in absorption test with water-saturated coating (**Abs-85W**) and it can be ascribed to the favorable repartition of toluene vapor in the hydrated ionic cluster channels of PFSA layer [96]: 14×10^{-6} s^{-1}(Fig. 5D). Photocatalytic degradation with the multilayered AQ-AD coating enhanced toluene disappearance,

and both tests in dry (**Pc-D**) and wet (**Pc-W**) conditions resulted more performing than the corresponding absorption, although not satisfying: k_{app} was 11×10^{-6} s^{-1} and 17×10^{-6} s^{-1}, respectively (Fig. 5D). The monitoring of toluene photocatalytic oxidation by GC-MS analysis of gas-phase samples detected benzene traces ascribable to decarboxylation of benzoic intermediates (eq. 12). Benzene easily back diffused from the AQ-AD photoactive coating to the reaction environment due to its extremely low affinity toward the PFSA-based catalytic layer. Benzene detection indirectly confirmed the formation of intermediates such as the aforementioned benzaldehyde and benzoic acid during the photocatalytic process by direct oxidation; however, these compounds were mainly retained in the AQ ionic clusters because of their polar interactions. Deactivation effects of the photocatalyst due to adsorption of benzoic acid, that is a recognized TiO_2 poisoning agent, were not observed [97, 98]. It is reasonable to assume that the ionomeric polymer of the photoactive coating played a role as protective layer. However, further insights are required on this specific subject. In wet conditions, it was also expected that hydroxylated benzaldehydes, which are characterized by high permeation in the PFSA layer, were synthesized through the hydroxyl radical-mediated oxidation of toluene.

Numerous methods are reported in literature addressing the degradation of chlorinated pollutants, whose permeation into PFSA membranes is however expected to be negligible [99-102]. A study by Sun *et al.* mentions the application of a PSFA coating in an electrocatalytic system for the abatement of chlorinated phenols [103]. The use of the multilayered AQ-AD photoactive coating to degrade chlorinated pollutants was thus considered for benchmarking purposes, and dichloromethane, CH_2Cl_2, was chosen because it is a widespread compound that finds many uses in industrial products and processing, such as aerosols, adhesives, dry cleaning, pharmaceuticals, refrigerants, and solvents [104]. In the gas-phase photooxidation of dichloromethane, the main

products of complete mineralization are hydrogen chloride, HCl, and carbon dioxide, CO_2 (eq. 14) [104,105]:

$$CH_2Cl_2 + O_2 \rightarrow CO_2 + 2\ HCl \qquad (14)$$

Carbonyl dichloride (*i.e.* phosgene), $COCl_2$, carbon monoxide, CO, elemental chlorine, Cl_2, carbon tetrachloride, CCl_4, and chloroform, $CHCl_3$, are also generated as intermediates or side-products [104,105]. Moreover, it is diffusely accepted that the conversion of dichloromethane by photodegradation decreases with an increase in water vapor concentration, because of a competitive adsorption on the active sites of the photocatalyst [100,104-106]. Dichloromethane absorption was negligibly improved upon hydration of the PFSA-based coating: in dry conditions at room temperature (**Abs-RTD**) a k_{app} equal to 4.8×10^{-6} s^{-1} was measured, which slightly increased to 5.4×10^{-6} s^{-1} in wet conditions at 85°C (**Abs-85W**) (Fig. 5E). In the photocatalytic degradation of dichloromethane through the multilayered AQ-AD photoactive coating the detrimental effects ascribable to water vapor were not observed, probably owing to the very low degradation obtained in all conditions, and a minimal increase in the photocatalytic rate was detected: the apparent kinetic constants in dry (**Pc-D**) and wet (**Pc-W**) conditions were equal to 6.6×10^{-6} and 7.1×10^{-6} s^{-1}, respectively (Fig. 5E). The PFSA-based phase surrounding TiO_2 particles covered the active sites of the photocatalyst, presumably minimizing the competitive adsorption between water and pollutant. Overall, dichloromethane showed the lowest values of photoabatement rates: it thus resulted significantly resistant to photocatalyzed oxidation, in particular to the oxidative process involving TiO_2 surface-adsorbed hydroxyl radicals. In fact, the improvement in **Pc-W** kinetics with respect to **Pc-D** is analogous to that observed passing from dry to wet absorption, and is therefore to ascribe to an improved absorption rather than to an enhanced photocatalytic mechanism.

Pyridine, being a proton acceptor with high proton affinity, easily interacts with the superacidic groups of PFSA membranes [107]. Buzzoni *et al.* studied the absorption of pyridine on dehydrated PFSA membranes, assessing that the following reaction (eq. 15) occurs even in dry conditions [107]:

$$R_F\text{–}SO_3H + Py \rightarrow (R_F\text{–}SO_3^{-}\cdots{}^{+}HPy) \qquad (15)$$

Decomposition of pyridine has been widely studied because this aromatic nitrogenated heterocycle, despite representing a serious hazard for human organs, is broadly used as industrial solvent and is present as building block in a large number of common fine chemicals, agrochemicals, and pharmaceuticals [108-112]. Several researches reported its decomposition by pyrolysis as well as by biodegradation [107, 111-117]. More recently, TiO_2 heterogeneous photocatalysis has been considered for pyridine mineralization (eq. 16) [107, 111-117]:

$$C_5H_5N + (25 + 2\,x)/4\ O_2 \rightarrow 5\ CO_2 + 5/2\ H_2O + NO_x \qquad (16)$$

Pyridine abatement with the multilayered AQ-AD photoactive coating was studied and the absorption of pyridine in the dehydrated as well as hydrated PFSA-based component of the coating was evaluated (Fig. 5F): the apparent kinetic rate constants in dry conditions at room temperature (**Abs-RTD**) and in wet conditions at 85°C (**Abs-85W**) were 27×10^{-6} s^{-1} and 32×10^{-6} s^{-1}, respectively. Due to the proton acceptor properties and the high proton affinity of pyridine, the interactions between this pollutant and the superacidic groups of PFSA membranes resulted facilitated by hydration of the AQ component of the photoactive coating. In the presence of the dehydrated PFSA-based coating, pyridine was thus the pollutant with the highest absorption rate, while in hydrated conditions it remained second only to methanol. a further decrease in concentration due to pyridine photocatalytic abatement was also observed in both dry (**Pc-D**) and wet (**Pc-W**) conditions at 85°C, showing k_{app} of 46×10^{-6} s^{-1} and 49×10^{-6} s^{-1}, respectively (Fig.

5F). It is worth noting that pyridine resulted the least stable pollutant toward photolytic abatement compared to the others: k_{app} of pyridine photolysis (**Pl**) was 19×10^{-6} s^{-1}.

4 Discussion

4.1 Mechanisms of coating-pollutant interaction and of photocatalytic degradation

Table 4 summarizes the results of absorption and degradation kinetics presented in the previous section.

Table 4. Absorption in dry (**Abs-RTD**) and wet conditions (**Abs-85W**) and photodegradation in dry (**Pc-D**) and wet conditions (**Pc-W**): kinetic constant, k_{app} ($\times 10^{-6}$ s^{-1}), and mechanism proposed.

Name	Abs-RTD	Abs-85W	Pc-D	Pc-W	Affinity to coating	Prevailing mechanism
Pentane	9.6	9.8	10	30	Low, not influenced by humidity	Dry and wet: indirect oxidation at coating-atmosphere interface
Methanol	23	54	144	171	High, enhanced by humidity	Dry: direct oxidation on TiO_2 Wet: both direct and indirect oxidation
2-propanol	14	80	*473**	157	High, enhanced by humidity	Dry: dehydration of 2-propanol in dry conditions (false positive) Wet: direct oxidation on TiO_2
Toluene	3	14	11	17	Low, enhanced by humidity	Dry: direct oxidation Wet: indirect oxidation
Dichloro-methane	4.8	5.4	6.6	7.1	Low, not influenced by humidity	Dry and wet: direct oxidation
Pyridine	27	32	46	49	High, low influence of humidity	Dry and wet: direct oxidation

The first consideration concerns the immobilization system proposed: indeed, the use of the multilayered AQ-AD photoactive coating overall enhanced the abatement of all the pollutants with respect to single layers, as shown in the preliminary characterization of the coating, particularly in conditions of water oversaturation, which allowed the hydration of the PFSA-based layer. As mentioned in the introduction section, few works in literature present proper photocatalyst immobilization systems and characterize their gas-phase activity; the majority of works are more simply spreading TiO_2 slurries by brush on a substrate. Yet, this practice is not satisfactory, as it poses the issue of nanoparticles dispersion in air, with all health hazards associated. Results here reported present an interesting progress of current photocatalytic systems, because a reliable immobilization method is proposed, which at the same time allows to reach photocatalytic reaction rates comparable to those found in literature for spread coatings [48,87,89].

Concerning the kinetics observed and the mechanisms envisioned, photolysis, direct oxidation and hydroxyl radical-mediated reaction were recognized as predominant routes in the photodegradation process of the pollutants.

Photolysis is unavoidable but it generally provided a rather negligible contribution to the catalyzed processes: only for dichloromethane abatement, the photolytic rate was almost half (around 56%) of the highest photocatalysis apparent kinetic constant.

Direct oxidation was facilitated for pollutants which easily migrate into the PFSA-layer containing the TiO_2 particles. Furthermore, on the hydrated coating the hydroxyl radical-mediated reactions could also occur, and were particularly relevant when the contact between pollutant and photocatalyst was hindered, *i.e.*, in presence of unfavorable PFSA coating-pollutant interactions,

as better described in next section. Hence, humidity proved its importance in stimulating photocatalysis by activating hydroxyl radical-mediated reactions which can occur in absence of direct contact of the pollutant with the photocatalyst, or in combination with direct oxidation paths improving the overall efficiency.

In this respect, not only photocatalysis, but also the absorption of pollutants through the ionomer layer seemed to be generally aided by hydration of the coatings: this is particularly true for toluene, whose absorption kinetic constant in dry atmosphere coincides with that for photolysis, therefore indicating a negligible absorption of the pollutant, while in the hydrated coating a 5-fold increase in absorption was obtained. Exception to this behavior are pentane and dichloromethane, which remained recalcitrant to absorption, although coating hydration increased pentane photocatalytic reaction rate – as abovementioned, this should be ascribed to the onset of an indirect photodegradation mechanism, where TiO_2-generated hydroxyl radicals migrate to the outer surface of the coating and come into direct contact with the pollutant. Absorption significantly influenced the abatement process because it represents the initial step in which pollutants migrate toward TiO_2 photocatalyst nanoparticles. Indeed, where absorption was high, also photocatalysis was more efficient, while in absence of absorption photocatalytic degradation resulted very low. This indicates that indirect oxidation at the coating-atmosphere interface is not sufficient to produce a significant pollutant degradation: the cause of this lies in the small contact area, rather than in the weakness of the indirect oxidation mechanism, which conversely is known to be vital to improve photocatalytic efficiency.

The previous considerations highlight the importance of the interactions between each single pollutant and the PFSA coating proposed as immobilization method for TiO_2: indeed, the chemical nature of the coating determines the likelihood of pollutants absorption, and therefore – as proved

above – of an efficient degradation, on the basis of their characteristics, most notably polarity and proticity, as highlighted in next paragraph.

4.2 Effect of pollutant polarity

The investigated pollutants can be classified on the basis of their polarity and their protic behavior: pentane and toluene are apolar and nearly apolar, respectively; dichloromethane is aprotic and weakly polar; methanol and 2-propanol are both protic and polar; pyridine is markedly polar with the nitrogen atom featuring a basic lone electron pair. In Figure 6 the apparent kinetic rate constants of absorption and photocatalytic tests performed by using hydrated coatings (**Abs-85W** and **Pc-W**) are plotted against the molecular dipole moment (expressed in Debye) of the corresponding pollutant.

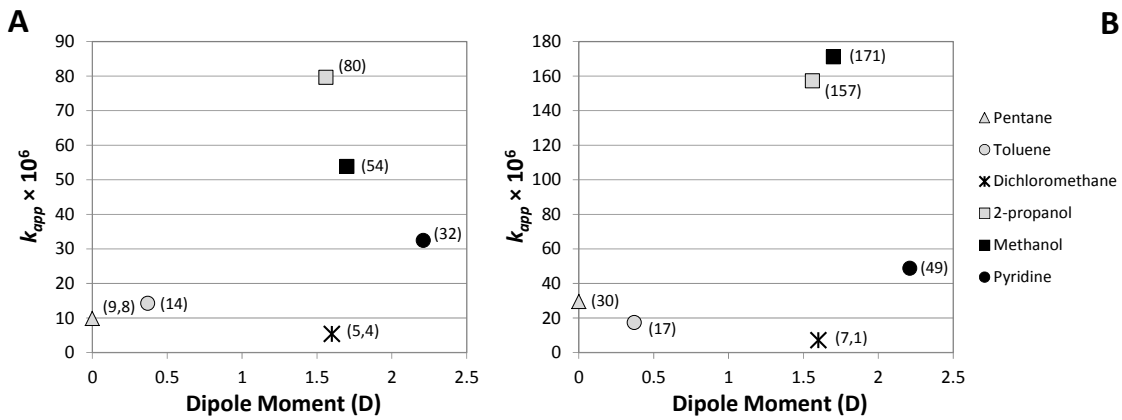

Figure 6. Absorption (A) and photocatalysis (B) rates in the presence of hydrated coating, plotted against the molecular dipole moment of pollutants. Apparent rate constant values (k_{app}) are reported in brackets (values × 10^{-6} s^{-1}).

Apolarity and aproticity resulted as main features at the base of low absorption and photocatalytic rates; the fastest kinetics were observed on two alcohols, *i.e.*, 2-propanol and methanol. In this respect, a trend inversion can be observed for the two alcoholic pollutants moving from absorption to photocatalysis: 2-propanol was absorbed more readily than methanol, but photodegradation of the latter exploited faster kinetics. This phenomenon can be ascribed to the overall efficiency of the methanol oxidation process, which took advantage of both direct and hydroxyl radical-mediated routes. Pyridine also showed good absorption and photodegradation rates that resulted from the balance between high polarity and Lewis-base features of its nitrogen atom.

The reason for the general behavior highlighted here is related to the chemical characteristics of the PFSA coating, whose polar heads and superacidic character push interactions with pollutants characterized by marked polarity and proticity and capability of hydrogen bonding, such as the alcoholic compounds like methanol and 2-propanol; this in turn enhanced their absorption and subsequent degradation. Hence, to exploit at maximum the advantages of the immobilization system proposed, the preliminary evaluation of the characteristics of pollutants to be degraded is recommended, to envision their possible interactions with the PFSA coating.

5 Conclusions

This work was aimed at providing a clear understanding of the photocatalytic activity of a perfluoropolymeric TiO_2-containing coating toward a selection of pollutants typical of indoor environments. The assessment involved the characterization of the coating absorption and photocatalytic efficiency in different relative humidity conditions, in order to have a better picture of its potential activity and of atmospheric conditions that enhance it. The intrinsic chemical nature of each pollutant was commented in regard to its influence on the absorption and photocatalytic

reaction rates. Protic compounds were found more prone to absorption in the coating and therefore subject to a faster degradation compared to aprotic ones. Polarity also aided the interaction of pollutant molecules with the coating, increasing their absorption rates, although to a lesser extent. Absorption facilitates pollutants mineralization owing to the multiplication of possible reaction pathways, since not only the molecules can react with oxidizing species created by TiO_2 and diffusing into the coating, but also with TiO_2 particles themselves. It is then possible to conclude that the immobilization system proposed can provide excellent gas phase photocatalytic activity towards polar and protic compounds thanks to enhanced interactions with the ionomer-based perfluorinated coating, reaching reaction kinetics comparable to those obtained with current testing systems, where immobilization is not properly achieved. To our knowledge, it is the first example of efficient gas-phase VOC degradation system where TiO_2 is embedded in a polymeric coating. These conclusions can be used as guidelines for the design of atmospheric purifiers based on the technology presented.

References

1. T. Salthammer, E. Uhde, Organic indoor air pollutants, 2nd Ed., Wiley-VCH, Weinheim, 2009.

2. Science Advisory Board - U.S. Environmental Protection Agency, Reducing risk: setting priorities and strategies for environmental protection, Washington, DC, 1990.

3. J.F. Argacha, T. Bourdrel, P. van de Borne, Ecology of the cardiovascular system: a focus on air-related environmental factors. Trends Cardiovas. Med. 28 (2018) 112-126.

4. T. Salthammer, Release of organic compounds and particulate matter from products, materials, and electrical devices in the indoor environment, in: P. Pluschke, H. Schleibinger (Eds.),

Handbook of environmental chemistry, vol. 64: indoor air pollution, Springer-Verlag Berlin Heidelberg, 2018, pp. 1-36.

5. M. Marć, M. Śmiełowska, J. Namieśnik, B. Zabiegała, Indoor air quality of everyday use spaces dedicated to specific purposes - a review. Environ. Sci. Pollut. Res. 25 (2018) 2065-2082.

6. F.W. Lipfert, Long-term associations of morbidity with air pollution: a catalog and synthesis. J. Air Waste Manage. Assoc. 68 (2018) 12-28.

7. J. Auvinen, L. Wirtanen, The influence of photocatalytic interior paints on indoor air quality. Atmos. Environ. 42 (2008) 4101-4112.

8. L. Mu, L. Liu, R. Niu, B. Zhao, J. Shi, Y. Li, W. Scheider, J. Su, S-C. Chang, S. Yu, Z-F. Zhang, Indoor air pollution and risk of lung cancer among chinese female non-smokers. Cancer Causes Control 24 (2013) 439-450.

9. G. Liu, M. Xiao, X. Zhang, C. Gal, X. Chen, L. Liu, S. Pan, J. Wu, L. Tang, D. Clements-Croome, A review of air filtration technologies for sustainable and healthy building ventilation. Sustain. Cities Soc. 32 (2017) 375-396.

10. H. Destaillats, W. Chen, M.G. Apte, N. Li, M. Spears, J. Almosni, G. Brunner, J.J. Zhang, W.J. Fisk, Secondary pollutants from ozone reactions with ventilation filters and degradation of filter media additives. Atmos. Environ. 45 (2011) 3561-3568.

11. A. Luengas, A. Barona, C. Hort, G. Gallastegui, V. Platel, A. Elias, A review of indoor air treatment technologies. Rev. Environ. Sci. Biotechnol. 14 (2015) 499-522.

12. A. Berenjian, N. Chan H. Jafarizadeh Malmiri, Volatile organic compounds removal methods: a review. Am. J. Biochem. Biotechnol. 8 (2012) 220-229.

13. M. Bahri, F. Haghighat, Plasma-based indoor air cleaning technologies: the state of the art-review. Clean Soil Air Water 42 (2014) 1667-1680.

14. S. Wang, H.M. Ang, M.O. Tade, Volatile organic compounds in indoor environment and photocatalytic oxidation: state of the art. Environ. Int. 33 (2007) 694-705.

15. D.T. Tompkins, M.A. Anderson, Evaluation of photocatalytic air cleaning capability: a literature review & engineering analysis; Final report. American Society of Heating, Refrigerating and Air Conditioning Engineers, Atlanta, GE, 2003.

16. A.H. Mamaghani, F. Haghighat, C-S. Lee, Photocatalytic oxidation technology for indoor environment air purification: the state-of-the-art. Appl. Catal. B: Environ. 203 (2017) 247-269.

17. Y. Boyjoo, H. Sun, J. Liu, V.K. Pareek, S. Wang, A review on photocatalysis for air treatment: From catalyst development to reactor design. Chem. Eng. J. 310 (2017) 537-559.

18. L. Zhong, F. Haghighat, Photocatalytic air cleaners and materials technologies - Abilities and limitations. Build. Environ. 91 (2015) 191-203.

19. B.E.S. Sanabria, A. Strini, L. Schiavi, A. Li Bassi, V: Russo, B. Del Curto, M.V. Diamanti, MP. Pedeferri, Photocatalytic activity of nanotubular TiO2 films obtained by anodic oxidation: A comparison in gas and liquid phase. Materials 11 (2018) 488.

20. M. Chen, J. Yao, Y. Huang, H. Gong, W. Chu, Enhanced photocatalytic degradation of ciprofloxacin over Bi2O3/(BiO)2CO3 heterojunctions: Efficiency, kinetics, pathways, mechanisms and toxicity evaluation. Chem. Eng. J. 334 (2018) 453-461.

21. Y. Huang, Y. Gao, Q. Zhang, Y. Zhang, J. Cao, W. Ho, S.C. Lee, Biocompatible FeOOH-Carbon quantum dots nanocomposites for gaseous NOx removal under visible light: Improved charge separation and High selectivity. J. Hazard. Mater. 354 (2018) 54-62.

2223. J. Schneider, M. Matsuoka, M. Takeuchi, J. Zhang, Y. Horiuchi, M. Anpo, D.W. Bahnemann, Understanding TiO_2 photocatalysis: mechanisms and materials. Chem. Rev.114 (2014) 9919-9986.

24. M.A. Henderson, A surface science perspective on TiO_2 photocatalysis. Surf. Sci. Rep. 66 (2011) 185-297.

25. O. Carp, C.L. Huisman, A. Reller, Photoinduced reactivity of titanium dioxide. Prog. Sol. State Chem. 32 (2004) 33-177.

26. J. Li, H. He, C. Hu, J. Zhao, The abatement of major pollutants in air and water by environmental catalysis. Front. Environ. Sci. Eng. 7 (2013) 302-325.

27. J. Sun, X. Yan, K. Lv, S. Sun, K. Deng, D. Du, Photocatalytic degradation pathway for azo dye in TiO_2/UV/O_3 system: hydroxyl radical versus hole. J. Mol. Catal. A Chem. 367 (2013) 31-37.

28. G. Shan, S. Yan, R.D. Tyagi, R.Y. Surampalli, T.C. Zhang, Applications of nanomaterials in environmental science and engineering: a review. Pract. Period. Hazard Toxic. Radioact. Waste Manage. 13 (2009)110-119.

29. T. Leshuk, P. Everett, H. Krishnakumar, K. Wong, S. Linley, F. Gu, Mesoporous magnetically recyclable photocatalysts for water treatment. J. Nanosci. Nanotechnol. 13 (2013) 3127-3132.

30. J. Bogdan, A. Jackowska-Tracz, J. Zarzyńska, J. Pławińska-Czarnak, Chances and limitations of nanosized titanium dioxide practical application in view of its physicochemical properties. Nanoscale Res. Lett. 10 (2015) 57.

31. Z. Xing, J. Zhang, J., Cui, J. Yin, T. Zhao, J. Kuang, Z. Xiu, N. Wan, W. Zhou, Recent advances in floating TiO_2-based photocatalysts for environmental application. Appl. Catal. B Environ. 225 (2018) 452-467.

32. A.Y. Shan, T.I.M. Ghazi, S.A. Rashid, Immobilisation of titanium dioxide onto supporting materials in heterogeneous photocatalysis: a review. Appl. Catal. A 389 (2010) 1-8.

33. Y. Zhao, Y. Liu, Q. Xu, M. Barahman, A.M. Lyons, Catalytic, self-cleaning surface with stable superhydrophobic properties: printed polydimethylsiloxane (PDMS) arrays embedded with TiO_2 nanoparticles. ACS Appl. Mater. Interfaces 7 (2015) 2632-2640.

34. G. Jayanthi Kalaivani, S.K. Suja, TiO_2 (rutile) embedded inulin - A versatile bio-nanocomposite for photocatalytic degradation of methylene blue. Carbohyd. Polym. 143 (2016) 51-60.

35. J. Yun, J.S. Im, A. Oh, D-H. Jin, T-S. Bae, Y-S. Lee, H-I. Kim, pH-sensitive photocatalytic activities of TiO_2/poly(vinyl alcohol)/poly(acrylic acid) composite hydrogels. Mater. Sci. Eng. B 176 (2011) 276-281.

36. W. Fa, C. Gong, L. Tian, T. Peng, L. Zan, Enhancement of photocatalytic degradation of poly(vinylchloride) with perchlorinated iron(II) phthalocyanine modified nano-TiO_2. J. Appl. Polym. Sci. 122 (2011) 1823-1828.

37. C. Yang, C. Gong, T. Peng, K. Deng, L. Zan, High photocatalytic degradation activity of the polyvinyl chloride (PVC)-vitamin C (VC)-TiO_2 nano-composite film. J. Haz. Mater. 178 (2010) 152-156.

38. L. Zan, S. Wang, W. Fa, Y. Hu, L. Tian, K. Deng, Solid-phase photocatalytic degradation of polystyrene with modifiednano-TiO_2 catalyst. Polym. 47 (2006) 8155-8162.

39. C.L. Bianchi, S. Ardizzone, G. Cappelletti, G. Cerrato, W. Navarrini, M. Sansotera, Nanostructured TiO_2 modified by perfluoropolyethers: gas phase photocatalytic activity. J. Mater. Res. 25 (2010) 96-103.

40. F. Persico, M. Sansotera, M.V. Diamanti, L. Magagnin, F. Venturini, W. Navarrini, Effect of amorphous fluorinated coatings on photocatalytic properties of anodized titanium surfaces. Thin Solid Films 545 (2013) 210-216.

41. W. Navarrini, M.V. Diamanti, M. Sansotera, F. Persico, M. Wu, L. Magagnin, S. Radice, UV-resistant amorphous fluorinated coating for anodized titanium surfaces. Prog. Org. Coat. 74 (2012) 794-800.

42. F. Persico, M. Sansotera, C.L. Bianchi, C. Cavallotti, W. Navarrini, Photocatalytic activity of TiO_2-embedded fluorinated transparent coating for oxidation of hydrosoluble pollutants in turbid suspensions. Appl. Catal. B Environ. 170-171 (2015) 83-89.

43. A.Y. Shan, T.I.M. Ghazi, S.A. Rashid, Immobilisation of titanium dioxide onto supporting materials in heterogeneous photocatalysis: A review. Appl. Catal. A General 389 (2010) 1-8.

44. S. Singh, H. Mahalingam, P.K. Singh, Polymer-supported titanium dioxide photocatalysts for environmental remediation: A review. Appl. Catal. A General 462-463 (2013) 178-195.

45. C.S. Lugo-Vega, B. Serrano-Rosales, H. de Lasa, Immobilized particle coating for optimum photon and TiO_2 utilization in scaled air treatment photo reactors. Appl. Catal. B Environ. 198 (2016) 211-223.

46.L. Lopez, W.A. Daoud, D. Dutta, B.C. Panther, T.W. Turney, Effect of substrate on surface morphology and photocatalysis of large-scale TiO_2 films. Appl. Surf. Sci. 265 (2013) 162-168.

47. A.H. Mamaghani, F. Haghighat, C-S. Lee, Gas phase adsorption of volatile organic compounds onto titanium dioxide photocatalysts. Chem. Eng. J. 337(2018) 60-73.

48. A. Šuligoj, U.L. Štangar, A. Ristić, M. Mazai, D. Verhovšek, N.N. Tušar, TiO_2–SiO_2 films from organic-free colloidal TiO_2 anatase nanoparticles as photocatalyst for removal of volatile organic compounds from indoor air. Appl. Catal. B Environ. 184 (2016) 119-131.

49. C. Maillard-Dupuy, C. Guillard, H. Courbon, P. Pichat. Kinetics and products of the TiO_2 photocatalytic degradation of pyridine in water. Environ. Sci. Technol. 28 (1994) 2176-2183.

50. V. Jordanovskal, P. Naumov, B. Boyanov, R. Trijko. Kinetic study on the photo-catalytic degradation of pyridine in TiO_2 suspension systems. Catal. Today 93-95 (2004) 857-861.

51. C-Y. Hsu, H-C. Chiang, R-H. Shie, C-H. Ku, T-Y. Lin, M-J. Chen, N-T. Chen, Y-C. Chen, Ambient VOCs in residential areas near a large-scale petrochemical complex: Spatiotemporal variation, source apportionment and health risk. Environ. Pollut. 240 (2018) 95-104.

52. M. Ting, W. Yue-Si, J. Jie, W. Fang-Kun, W. Mingxing, The vertical distributions of VOCs in the atmosphere of Beijing in autumn. Sci. Total Environ. 390 (2008) 97-108.

53. Y. Huang, S.S.H. Ho, R. Niu, L. Xu, Y. Lu, J. Cao. Removal of indoor volatile organic compounds via photocatalytic oxidation: a short review and prospect. Molecules 21 (2016) 56(1-20).

54. C. He, W. Chen, K. Han, B. Guo, J. Pei, J.S. Zhang. Evaluation of performance: correlation between high and low challenge concentration tests for toluene and formaldehyde (ASHRAE RP-1557). HVAC&R Research 20 (2014) 508-521.

55. B. Ohtani, O.O. Prieto-Mahaney, D. Li, R. Abe, What is Degussa (Evonik) P25? Crystalline composition analysis, reconstruction from isolated pure particles and photocatalytic activity test. J. Photochem. Photobiol. A Chem. 216 (2010) 179-182.

56. A. Russo, W. Navarrini, Perfluoro-4-methyl-1,3-dioxole: a new monomer for high-T_g amorphous fluoropolymers. J. Fluorine Chem. 125 (2004) 73-78.

57. G. Colón, M.C. Hidalgo, J.A. Navío. Effect of ZrO_2 incorporation and calcination temperature on the photocatalytic activity of commercial TiO_2 for salicylic acid and Cr(VI) photodegradation. Appl. Catal. A 231 (2002) 185-199.

58. X. Zhang, H. Li, X. Lv, J. Xu, Y. Wang, C. He, N. Liu, Y. Yang, Y. Wang, Facile Synthesis of Highly Efficient Amorphous Mn□MIL□100 Catalysts: Formation Mechanism and Structure Changes during Application in CO Oxidation. Chem.-A European J. 24 (2018) 8822-8832.

59. Y. Yang, H. Dong, Y. Wang, C. He, Y. Wang, X. Zhang, Synthesis of octahedral like Cu-BTC derivatives derived from MOF calcined under different atmosphere for application in CO oxidation. J. Sol. State Chem. 258 (2018) 582-587.

60. R. Buzzoni, S. Bordiga, G. Ricchiardi, G. Spoto, A. Zecchina, Interaction of H_2O, CH_3OH, $(CH_3)_2O$, CH_3CN, and pyridine with the superacid perfluorosulfonic membrane Nafion: An IR and Raman study. J. Phys. Chem. 99 (1995) 11937-11951.

61. D.T. Hallinan, Jr., Y.A. Elabd, Diffusion and sorption of methanol and water in Nafion using time-resolved Fourier transform infrared-attenuated total reflectance spectroscopy. J. Phys. Chem. B 111 (2007) 13221-13230.

62. A. Fujishima, T.N. Rao, D.A. Tryk, Titanium dioxide photocatalysis. J. Photochem. Photobiol. C 1 (2000) 1-21.

63. C.L. Bianchi, S. Gatto, C. Pirola, A. Naldoni, A. Di Michele, G. Cerrato, V. Crocellà, V. Capucci, Photocatalytic degradation of acetone, acetaldehyde and toluene in gas-phase: Comparison between nano and micro-sized TiO_2. Appl. Catal. B Environ. 146 (2014) 123-130.

64. M. Marelli, C. Evangelisti, M.V. Diamanti, V. Dal Santo, M.P. Pedeferri, C.L. Bianchi, L. Schiavi, A. Strini, TiO_2 nanotubes arrays loaded with ligand-free Au nanoparticles: Enhancement in photocatalytic activity. ACS Appl. Mater. Interfaces 8 (2016) 31051-31058.

65. T.D. Gierke, W.Y. Hsu, The cluster-network model of ion clustering in perfluorosulfonated membranes, in: A. Eisenberg, H.L. Yeager (Eds.), Perfluorinatedionomer membranes, ACS Symposium series, American Chemical Society, Washington, DC, 1982, pp. 283-307.

66. K. Tadano, E. Hirasawa, H. Yamamoto, S. Yano, Order-disorder transition of ionic clusters in ionomers. Macromolecules 22 (1989) 226-233.

67. T. Yamaguchi, C.A. Koval, R.D. Noble, C.N. Bowman, Transport mechanism of carbon dioxide through perfluorosulfonate ionomer membranes containing an amine carrier. Chem. Eng. Sci. 51 (1996) 4781-4789.

68. W. Grot, Fluorinated ionomers, William Andrew Inc., Norwich, NY, 2008.

69. V. Arcella, P. Colaianna, P. Maccone, A. Sanguineti, A. Gordano, A study on a perfluoropolymer purification and its application to membrane formation. J. Membrane Sci. 163 (1999) 203-209.

70. P. Pichat, Photocatalysis and water purification: from fundamentals to recent applications, Wiley-VCH Verlag GmbH & Co. KGaG, Weinheim, 2013.

71. J. Shang, Y. Du, Z. Xu, Photocatalytic oxidation of heptane in the gas-phase over TiO_2. Chemosphere 46 (2002) 93-99.

72. A.K. Boulamanti, C.J. Philippopoulos, Photocatalytic degradation of C_5-C_7 alkanes in the gas-phase. Atmos. Environ. 43 (2009) 3168-3174.

73. C. Hartnig C. Roth, Polymer electrolyte membrane and direct methanol fuel cell technology, 1st Ed., Volume 2: In situ characterization techniques for low temperature fuel cells, Woodhead Publishing Ltd., Sawston (UK), 2012.

74. V.M. Barragán, C. Ruiz-Bauzá, J.P.G. Villaluenga, B. Seoane, Transport of methanol and water through Nafion membranes, J. Power Sources 130 (2004) 22-29.

75. D.T. Hallinan, Y.A. Elabd, Diffusion and sorption of methanol and water in Nafion using time-resolved fourier transform infrared-attenuated total reflectance spectroscopy, J. Phys. Chem. B 111 (2007) 13221-13230.

76. X. Ren, T.E. Springer, S. Gottesfeld, Water and methanol uptakes in Nafion membranes and membrane effects on direct methanol cell performance, J. Electrochem. Soc. 147 (2000) 92-98.

77. M.W. Verbrugge, methanol diffusion in perfluorinated ion-exchange membranes, J. Electrochem. Soc. 136 (1989) 417-423.

78. E. Skou, P. Kauranen1, J. Hentschel, Water and methanol uptake in proton conducting Nafion® membranes, Solid State Ionics 97 (1997) 333-337.

79. C.M. Gates, J. Newman, Equilibrium and diffusion of methanol and water in a Nafion 117 membrane, AIChE J. 46 (2000) 2076-2085.

80. X. Ren, T.E. Springer, T.A. Zawodzinski, S. Gottesfeld, Methanol transport through Nafion membranes electro-osmotic drag effects on potential step measurements, J. Electrochem. Soc. 147 (2000) 466-474.

81. D. Nandan, H. Mohan, R.M. Iyer, Methanol and water uptake, densities, equivalental volumes and thicknesses of several uni- and divalent ionic perfluorosulphonate exchange membranes (Nafion-117) and their methanol-water fractionation behaviour at 298 K, J. Memb. Sci. 71 (1992) 69-80.

82. M. Saito, S. Tsuzuki, K. Hayamizu, T. Okada, Alcohol and proton transport in perfluorinated ionomer membranes for fuel cells, J. Phys. Chem. B 110 (2006) 24410-24417.

83. M.A. Henderson, A surface science perspective on TiO_2 photocatalysis, Surf. Sci. Rep. 66 (2011) 185-297.

84. W.Z. Lang, W. Tong, Z.L. Xu, Preparation of PFSA-PVA/PSF hollow fiber membrane for IPA/H_2O pervaporation process, J. Appl. Polym. Sci. 108 (2008) 370-379.

85. P.P. Lu, Z.L. Xu, H. Yang, Y.M. Wei, H.T. Xu, Effects of ethanol and isopropanol on the structures and properties of polyethersulfone/perfluorosulfonic acid nanofibers fabricated via electrospinning, J. Polym. Res. 19 (2012) 9854.

86. M.J. Munoz-Batista, U. Caudillo-Flores, F. Ung-Medina, M. del Carmen Chávez-Parga, J.A. Cortés, A. Kubacka, M. Fernández-García, Gas phase 2-propanol degradation using titania photocatalysts: study of the quantum efficiency, Appl. Catal. B: Environ. 201 (2017) 400-410.

87. Y. Wang, H. Wang, X. Tan, Study of 2-propanol photocatalytic degradation on surface of phase-ratio-controlled TiO_2 nanoparticles, Trans. Tianjin Univ. 24 (2018) 1-7.

88. B. Neppolian, H. Yamashita, Y. Okada, H. Nishijima, M. Anpo, Preparation of TiO_2 photocatalysts by multi-gelation and their photocatalytic reactivity for the degradation of 2-propanol, Chem. Lett. 33 (2004) 268-269.

89. J. Arana, A. Pena Alonso, J.M. Dona Rodriguez, G. Colon, J.A. Navio, J. Perez Pena, FTIR study of photocatalytic degradation of 2-propanol in gas phase with different TiO_2 catalysts, Appl. Catal. B: Environ. 89 (2009) 204-213.

90. Z. Pengyi, L. Fuyan, Y. Gang, C. Qing, Z. Wanpeng, A comparative study on decomposition of gaseous toluene by O_3/UV, TiO_2/UV and O_3/TiO_2/UV. J. Photochem. Photobiol., A 156 (2003) 189-194.

91. A. Mills, C. O'Rourke, Photocatalytic oxidation of toluene in an NMR tube. J. Photochem. Photobiol., A 233 (2012) 34-39.

92. M. Muños-Batista, A. Kubacka, M.N. Gómes-Cerezo, D. Tudela, M. Fernández-García, Sunlight-driven toluene photo-elimination using CeO_2-TiO_2 composite systems: a kinetic study. Appl. Catal. B: Environ. 140-141 (2013) 626-635.

93. N. Itoh, W.C. Xu, S. Hara, K. Sakaki, Electrochemical coupling of benzene hydrogenation and water electrolysis. Catal. Today 56 (2000) 307-314.

94. C. Iwakura, Y. Tsuchiyama, K. Higashiyama, E. Higuchi, H. Inoue, Successive hydrogenation and dechlorination systems using palladized ion exchange membranes. J. Electrochem. Soc. 151 (2004) D1-D5.

95. S. Mitsushima, Y. Takakuwa, K. Nagasawa, Y. Sawaguchi, Y. Kohno, K. Matsuzawa, Z. Awaludin, A. Kato, Y. Nishiki, Membrane electrolysis of toluene hydrogenation with Water decomposition for energy carrier synthesis. Electrocatalysis 7 (2016) 127-131.

96. S.R. Poulson, R.R. Harrington, J.I. Drever, The solubility of toluene in aqueous salt solutions. Talanta 48 (1999) 633-641.

97. M.D. Hernández-Alonso, I. Tejedor-Tejedor, J.M. Coronado, M.A. Anderson, Operando FTIR study of the photocatalytic oxidation of methylcyclohexane and toluene in air over TiO2–ZrO2 thin films: Influence of the aromaticity of the target molecule on deactivation. Appl. Catal. B 101 (2011) 283-293.

98. S. Ardizzone, C.L. Bianchi, G. Cappelletti, A. Naldoni, C. Pirola, Photocatalytic Degradation of Toluene in the Gas Phase: Relationship between Surface Species and Catalyst Features. Environ. Sci. Technol. 42 (2008) 6671–6676.

99. C.-Y. Hsiao, C.L. Lee, D.F. Ollis, Heterogeneous photocatalysis: degradation of dilute solutions of dichloromethane (CH_2Cl_2), Chloroform ($CHCl_3$), and carbon tetrachloride (CCl_4) with illuminated TiO_2 photocatalyst. J. Catal. 82 (1983) 418-423.

100. M. Shestakova, M. Sillanpää, Removal of dichloromethane from ground and wastewater: a review. Chemosphere 93 (2013) 1258-1267.

101. S. Ozaki, L-H. Zhao, T. Amemiya, K. Itoh, M. Murabayashi, Gas-phase photocatalytic degradation of *cis*-1,2-dichloroethylene using titanium dioxide under near-UV-illumination. Appl. Catal. B: Environ. 52 (2004) 81-89.

102. M.A. Brusa, Y. Di Iorio, M.S. Churio, M.A. Grela, Photocatalytic air oxidation of cyclohexane in CH_2Cl_2/C_6H_{12} mixtures over TiO_2 particles: an attempt to rationalize the positive effect of dichloromethane on the yields of valuable oxygenates. J. Mol. Catal. A: Chem. 268 (2007) 29-35.

103. Z. Sun, X. Ma, X. Hu, Electrocatalytic dechlorination of 2,3,5-trichlorophenol on palladium/carbon nanotubes-nafion film/titanium mesh electrode. Environ. Sci. Pollut. Res. 24 (2017) 14355–14364.

104. J. Borisch, S. Pilkenton, M.L. Miller, D. Raftery, J.S. Francisco, TiO_2 Photocatalytic Degradation of Dichloromethane: An FTIR and Solid-State NMR Study. J. Phys. Chem. B 108 (2004) 5640–5646.

105. W.-C. Hung, S.-H. Fu, J.-J. Tseng, H. Chu, T.-H. Ko, Study on photocatalytic degradation of gaseous dichloromethane using pure and iron ion-doped TiO_2 prepared by the sol–gel method. Chemosphere 66 (2007) 2142–2151.

106. N.N. Lichtin, M. Avudaithai, TiO_2-Photocatalyzed Oxidative Degradation of CH_3CN, CH_3OH, C_2HCl_3, and CH_2Cl_2 Supplied as Vapors and in Aqueous Solution under Similar Conditions. Environ. Sci. Technol. 30 (1996) 2014–2020.

107. A.G. Agrios, P. Pichat, Recombination rate of photogenerated charges versus surface area: Opposing effects of TiO_2 sintering temperature on photocatalytic removal of phenol, anisole, and pyridine in water. J. Photochem. Photobiol. A: Chem. 180 (2006) 130–135.

108. C. Mailiard-Dupuy, C. Guillard, H. Courbon, P. Pichat, Kinetics and Products of the TiO_2 photocatalytic degradation of pyridine in water. Environ. Sci. Technol. 28 (1994) 2176-2183.

109. D. Ma, Y. Yan, H. Ji, C. Chen, J. Zhao, Photocatalytic activation of pyridine for addition reactions: an unconventional reaction feature between a photo-induced hole and electron on TiO_2. Chem. Commun. 51 (2015) 17451–17454.

110. R.R. Solís, F. Javier Rivas, O. Gimeno, J.L. Pérez-Bote, Photocatalytic ozonation of pyridine-based herbicides by N-doped titania. J. Chem. Technol. Biotechnol. 91 (2016) 1998–2008.

111. D.R. Stapleton, I.K. Konstantinou, D. Mantzavinos, D. Hela, M. Papadaki, On the kinetics and mechanisms of photolytic/TiO_2-photocatalytic degradation of substituted pyridines in aqueous solutions. Appl. Catal. B: Environ. 95 (2010) 100–109.

112. D.R. Stapleton, D. Mantzavinos, M. Papadaki, Photolytic (UVC) and photocatalyic (UVC/TiO_2) decomposition of pyridines. J. Haz. Mater. 146 (2007) 640–645.

113. H. Zhao, S. Xu, J. Zhong, X. Bao, Kinetic study on the photo-catalytic degradation of pyridine in TiO_2 suspension systems. Cat. Tod. 93–95 (2004) 857–861.

114. M.A. Aramendía, J.C. Colmenares, S. López-Fernández, A. Marinas, J.M. Marinas, J.M. Moreno, F.J. Urbano, Photocatalytic degradation of chlorinated pyridines in titania aqueous suspensions. Cat. Tod. 138 (2008) 110–116.

115. P. Kopf, E. Gilbert, S.H. Eberle, TiO_2 photocatalytic oxidation of monochloroacetic acid and pyridine: influence of ozone. J. Photochem. Photobiol. A: Chem. 136 (2000) 163–168.

116. P. Bhatt, M.S. Kumar, S. Mudliar, T. Chakrabarti, Biodegradation of Chlorinated Compounds—A Review. Crit. Rev. Environ. Sci. Technol. 37 (2007) 165–198.

117. S. Fetzner, Bacterial degradation of pyridine, indole, quinoline, and their derivatives under different redox conditions. Appl. Microbiol. Biotechnol. 49 (1998) 237–250.